Estimation of controllability region of unstable vertical plasma position and plasma separatrix multivariable reachability area of a spherical tokamak

Y.V. Mitrishkin[1, 2], V.I. Kruzhkov[1, 2], M.I. Patrov[3]

[1] *Lomonosov Moscow State University, Faculty of Physics, Moscow, Russia*
[2] *V.A. Trapeznikov Institute of Control Sciences of the RAS, Moscow, Russia*
[3] *Ioffe Institute of the Russian Academy of Sciences, St. Petersburg, Russia*

Spherical tokamaks are the most perspective devices for the commercially viable modular fusion power plant [1].The poloidal system of the spherical Globus-M tokamak (Ioffe Inst., S-Petersburg, RF) is shown in Fig. 1. Its plasma magnetic control system is presented in Fig. 2. In this scheme robust PID-controllers were tuned by the Quantitative Feedback Theory (QFT) [2]. The idea of this method is in Nichols chart analysis of an open loop system (Fig. 3). As result, PID-controllers and pre-filer (PF) were tuned with transfer functions as follows:

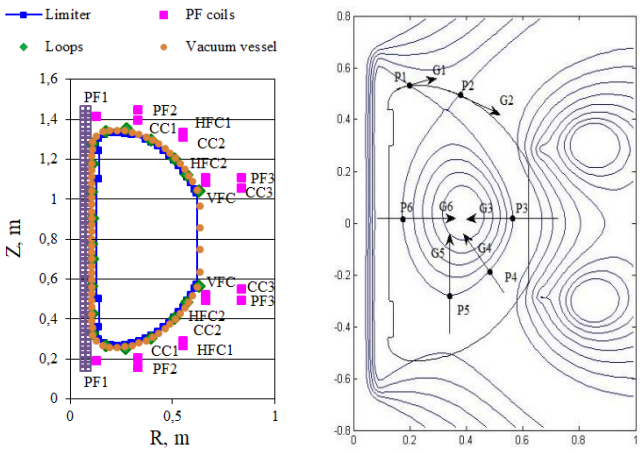

a) b)

Fig. 1. a) Poloidal system, b) equal level lines of poloidal magnetic flux in vertical cross-section of Globus-M and points *G*1-*G*6 for the gaps control.

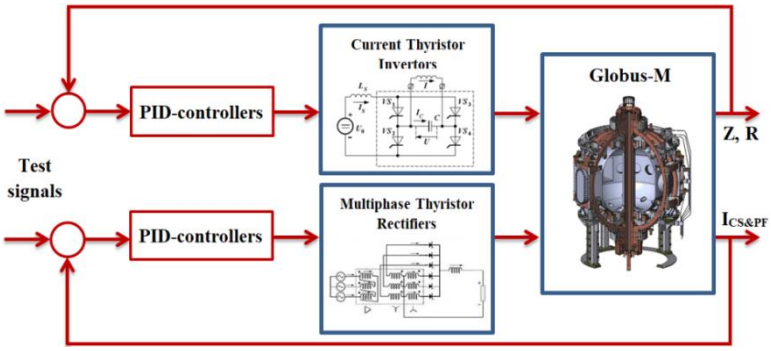

Fig. 2. Diagram of the Globus-M tokamak plasma control system.

$$\mathrm{PID}_Z(s) = 22.5\left(1+\frac{1}{0.0277s}+\frac{0.002s}{0.002s/94+1}\right),$$

$$\mathrm{PF}_Z(s) = \frac{10^3}{s+10^3},$$

$$\mathrm{PID}_R(s) = 30\left(1+\frac{1}{0.03s}+\frac{1.9\times10^{-3}s}{1.9\times10^{-3}s/1.7+1}\right).$$

Step responses of the control systems of *R* and *Z* with these controllers and *full* nonlinear self-oscillations models of thyristor Current Inverters (CI) [3] as actuators are shown in Fig. 3b. After PID-controllers were tuned, the estimation of the vertical controllability region [4] was done considering the restriction of the voltage on the vertical plasma position control coil: $|u| < u_{\max} = 900V$. The scheme with the tuned horizontal position (*R*) PID-controller and without the vertical position (*Z*) control loop was used for the estimation. The analytical estimation of the controllability region was done with the help of the state-space model:

$$\dot{x} = Ax + Bu,\ Z = Cx, \qquad x \in R^{40},\ u \in R^1, Z \in R^1;\ \ |u| < u_{\max}.$$

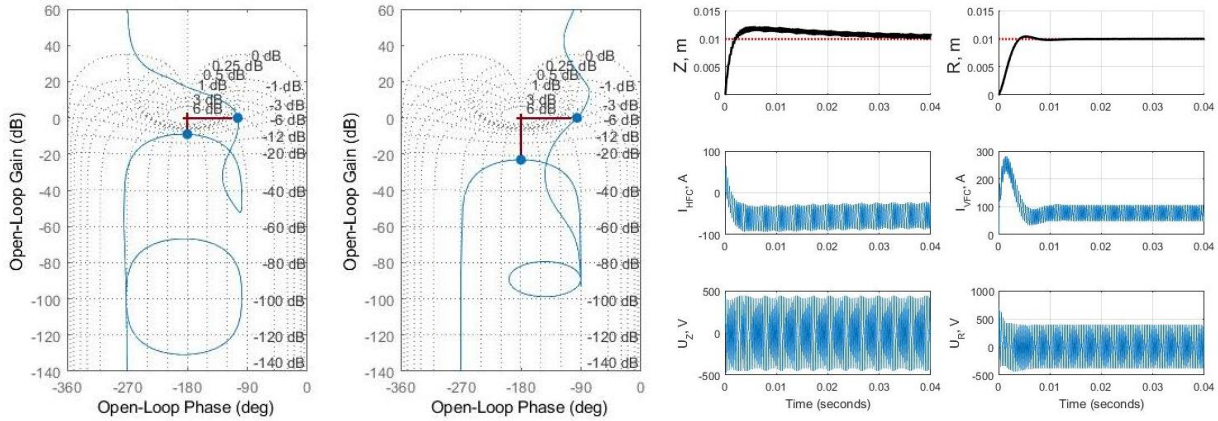

a) b)

Fig. 3. a) Nichols charts of the open-loop systems tuned by the QFT approach. The left chart is for the vertical plasma position *Z* control system, the right chart is for the horizontal plasma position *R* control system. Phase margins are equal to 75.5^0; 83.9^0, amplitude margins are 9.09 dB; 23.1 dB. b) Step responses of the vertical and horizontal plasma positions with PID-controllers tuned by the QFT approach and with full nonlinear CI models.

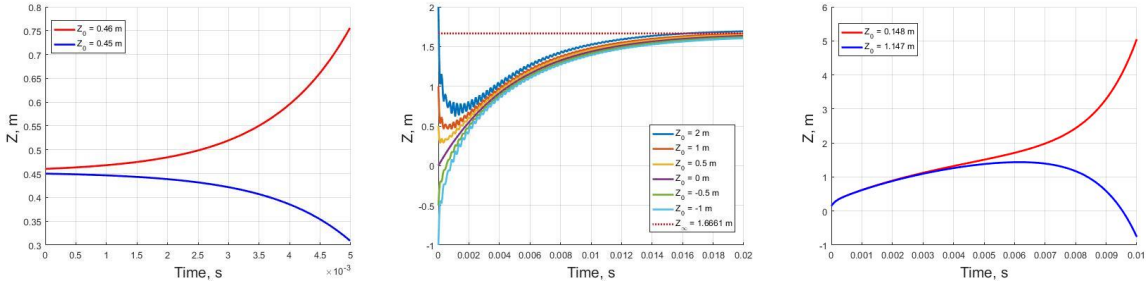

a) b) c)

Fig. 4. a) Dynamics of the unstable subsystem with different initial displacements; b) dynamics of the stable subsystem with different initial displacements; c) dynamics of the whole system in the numerical simulations with different initial displacements.

For the analytical analysis of the system the transfer to a new basis was done to separate stable and unstable parts of the system and get the restriction on the state in the new basis: $|\hat{x}_{22}|_{\max} < |\hat{b}_{22}||u|_{\max}/\lambda_{22} = 1.9383\times10^4$. Estimations $\hat{x}_{22}(0) = 1.3146\times10^5 Z_0$, $|Z_0| < 0.1477\,m$ were obtained by using the relation between 'new' and 'old' bases. The maximum initial vertical displacement that might be parried by maximum voltage value on the control coil was obtained by numerical simulations (Fig. 4) [4]. Numerical and analytical results are equal.

Then the plasma shape reachability area in a steady-state regime was estimated considering current restrictions of control coils. For this, the matrix relation between inputs and outputs was received: $y = Mu$. Inputs u are the setpoints of Z and R displacements and setpoints of currents of control coils. Outputs y are the projections of plasma shape points to selected directions (Fig. 1b). Plasma dynamics is described by the equations: $\dot{x} = Ax + Bu$, $y = Cx$. In the steady-state regime $\dot{x} = 0$ hence $x = -A^{-1}Bu$, $y = -CA^{-1}Bu$, and $M = -CA^{-1}Bu$. Two estimations were calculated using this relation: upper and lower ones. There are no shapes beyond the upper estimation because of the given limits and there are any shapes inside the

lower estimation. For calculation of the upper estimation the inputs with maximum values and needed signs were used (Fig. 5a). For calculation of the lower estimation a previously auxiliary estimation was obtained (Fig. 5 b). The auxiliary estimation is the maximum $y_{i\max}$ of each plasma shape point projection y_i with all other projections equal zero. As a result $y_{\max} = [y_{1\max} ... y_{6\max}]^T$ where $y_{i\max}$ is the maximum in the vector $[0...y_{j\max}...0]^T = Mu^{(j)}$ with $u^{(j)} = [u_1^{(j)} ... u_8^{(j)}]^T : |u_i^{(j)}| < u_{i\max}$. The index j for $u^{(j)}$ corresponds to $y_{j\max}$, $j = 1,...,6$. For calculation of $y_{i\max}$ the matrix M was decomposed into two matrices $M_1 \in R^{6x2}$ and $M_2 \in R^{6x6} : M = [M_1\ M_2]$, then $[0...y_{j\max}...0]^T = [M_1\ M_2]\left[u_1^{(j)} ... u_8^{(j)}\right]^T$, $[u_3^{(j)} ... u_8^{(j)}]^T = = M_2^{-1}([0...y_{j\max}...0]^T - M_1[u_1^{(j)}\ u_2^{(j)}]^T)$. The value $y_{i\max}$ was obtained using binary search.

One sixth of the auxiliary estimation is the lower estimation because the plasma model is linear (Fig. 5 c). Let us the output vector $Y = [y_1 ... y_6]^T$ where $|y_i| \le y_{i\max}/6$, $i = 1,...,6$. Then

$$Y = [y_1\ 0...0]^T + ... + [0...0\ y_6]^T \le ([y_{1\max}\ 0...0]^T + ... + [0...0\ y_{6\max}]^T)/6 =$$

$$= M([u_1^{(1)} ... u_8^{(1)}]^T + ... + [u_1^{(6)} ... u_8^{(6)}]^T)/6 \le M([u_{1\max} ... u_{8\max}]^T + ... + [u_{1\max} ... u_{8\max}]^T)/6 =$$

$$= M[u_{1\max} ... u_{8\max}]^T, \text{ thus } Y \le M[u_{1\max} ... u_{8\max}]^T.$$ So Y can be gotten using allowable inputs.

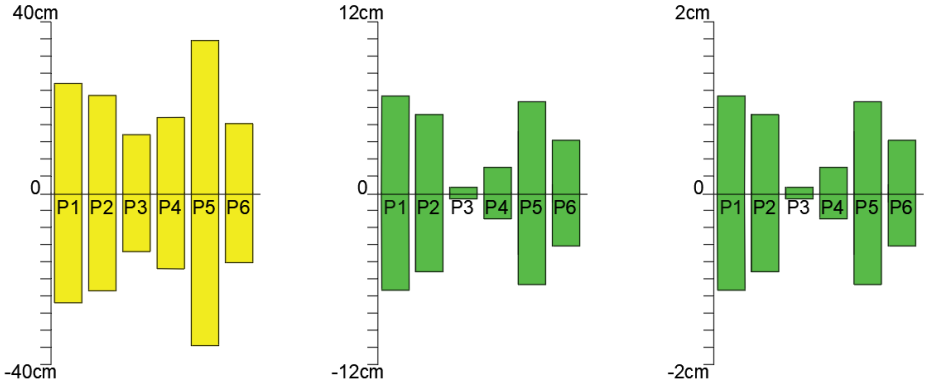

Fig. 5. a) Upper, b) auxiliary and c) lower estimations of the plasma separatrix reachability area at 8 inputs and 6 outputs.

In addition, the controllability region was obtained on state-space projections to the (*I*, *Z*)-plane. This estimation was done by two approaches: analytical with the use of the 2-order simplified model of the plasma in the tokamak and numerical one. Simplistically the tokamak is the series connection of the coil and the plasma, which may be described by stable and unstable first-order transfer functions respectively (Fig. 6). Using identification approach [5] to the closed-loop control system by means of MatLab, parameters of the system units (Fig. 6,

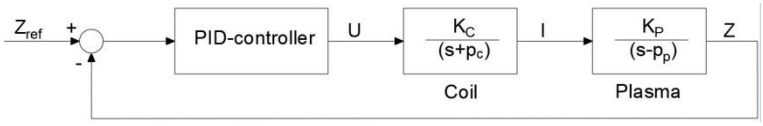

Fig. 6. Block-diagram of the 2-order closed-loop system.

7a) were obtained: $K_c = 2668.3\ A/V$, $p_c = 297.7274\ s^{-1}$; $K_p = 0.1536$ m/A, $p_p = 761.7\ s^{-1}$. The simplified 2-order differential equation of the control system was integrated:

$$Z(t, I_0, Z_0) = K_p \frac{(K_c U - p_c I_0)e^{-p_c t} - (p_c + p_p)K_c U + (K_c K_p U + K_p p_p I_0 + Z_0 p_c p_p + Z_0 p_p^2)e^{p_p t}}{p_c(p_c + p_p)},$$

$I(t, I_0) = (K_c U - e^{-p_c t})(K_c U - p_c I_0))/p_c$, the relation between Z and I, I_0, Z_0 was obtained:

$$Z(I, I_0, Z_0) = -\frac{K_p}{p_c}\left(\frac{K_c U}{p_p} + \frac{p_c I - K_c U}{p_c + p_p}\right) + \frac{(K_p(K_c U + p_p I_0) + Z_0 p_p(p_c + p_p))(p_c I_0 - K_c U)}{p_p(p_c + p_p)(p_c I - K_c U))^{(s2/s1)}}.$$

From where the asymptotes of the dynamics of $Z(I)$ were derived on the phase plane: $Z(I) = -\frac{K_p}{p_c}\left(\frac{K_c U}{p_p} + p_c I - K_c U\right)/(p_c + p_p)$ and $I = K_c U / p_c$, where $U = \pm U_{\max}$. These asymptotes are the bounds of the controllability region. The 2-order system is not able to describe the dynamics of the full 24-order system at relatively large deviations precisely. Numerical simulations of the open-loop full-order system with the maximum control voltage have showed that controllability region is less than the region predicted by the 2-order system: $Z(I) = -1.780 \times 10^{-4} I \pm 0.146$ (Fig.7b) [6]. The numerical estimation is more precise at large deviations because it takes into account all the model states.

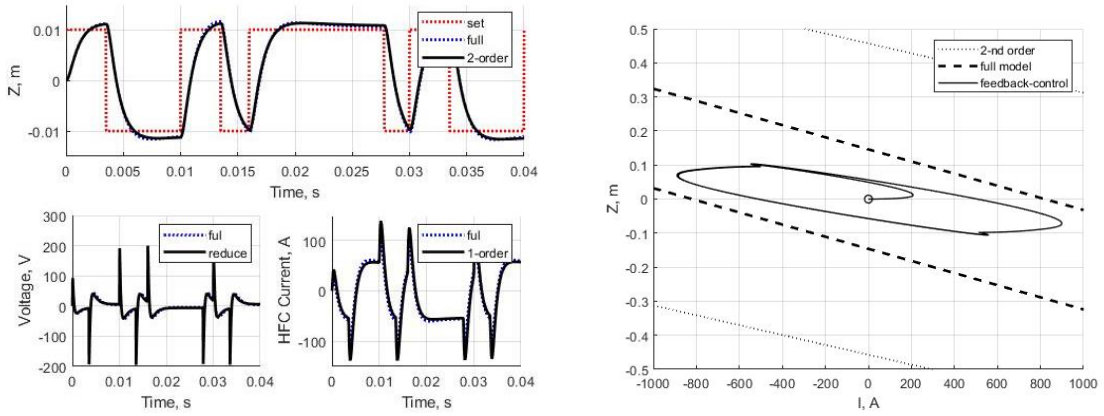

a) b)

Fig. 7. a) Processes in the closed-loop control system with full and second-order plant models; b) state-space projections and controllability regions for the full and second-order system.

This work was supported by the RSF, grant № 17-19-01022, and the RFBR, grant № 17-08-00293.

References

[1] Chuyanov V.A., Gryaznevich M.P. Fusion Engineering and Design, 2017, vol. 122, pp. 238-252.

[2] Garcia-Sanz M. Robust Control Engineering. Practical QFT solutions. Taylor & Francis Group, 2017.

[3] Kuznetsov E.A., Mitrishkin Y.V., Kartsev N.M. Fusion Eng. and Design, 2019, vol. 143, pp. 247-258.

[4] Humphreys D.A., Casper T.A., Eidietis N., Ferrara M., Gates D.A., et al. Nucl. Fusion 2009, vol. 49.

[5] Ljung L. System Identification. Theory for the User. Prentice Hall PTR, 1999.

[6] Mitrishkin Y.V. Plasma Devices and Operations, 1995, Vol. 4, pp. 111-140.